Journal of Materials Chemistry

Cite this: *J. Mater. Chem.*, 2012, **22**, 6419

www.rsc.org/materials

PAPER

Colour tuning from green to red by substituent effects in phosphorescent tris-cyclometalated iridium(III) complexes of carbazole-based ligands: synthetic, photophysical, computational and high efficiency OLED studies†

Mustafa Tavasli,[a] Tom N. Moore,[b] Yonghao Zheng,[b] Martin R. Bryce,*[b] Mark A. Fox,[b] Gareth C. Griffiths,[c] Vygintas Jankus,[c] Hameed A. Al-Attar[c] and Andrew P. Monkman[c]

Received 7th October 2011, Accepted 10th February 2012
DOI: 10.1039/c2jm15049b

Two series of *fac*-tris-cyclometalated iridium(III) complexes, series **1** from the 2-(carbazol-3′-yl)-pyridine ligands, and series **2** from the isomeric 2-(carbazol-2′-yl)-pyridine ligands, have been characterised. The photoluminescence and electroluminescence from series **2** complexes are red shifted compared to series **1** complexes, due to the increased electron donating ability of the carbazole unit in series **2**. The attachment of trifluoromethyl and methoxy substituents to the pyridyl ring in these complexes results in colour tuning of phosphorescence energy maxima over the range 494–637 nm (green to red). These complexes possess predominantly ^{3}MLCT (metal-to-ligand-charge transfer) excited states. DFT/TD-DFT computations correctly predict the phosphorescence emission maxima and show that the HOMOs in these complexes contain mixed iridium and carbazolyl character. The carbazolyl ligand contributions to the excited states increase in series **2** compared to series **1**. Complexes of series **1** exhibit high phosphorescence quantum yields whereas complexes of series **2** show lower quantum yields. Solution processed organic light emitting devices (OLEDs) with series **1** complexes using the high triplet poly(9-vinylcarbazole) (PVK) as the host polymer exhibit very high performances of up to 40 cd A^{-1} and external quantum efficiency of 12%. For series **2** the highest current efficiency is 10.3 cd A^{-1} and external quantum efficiency of 5.6%.

Introduction

Homoleptic and heteroleptic cyclometalated Ir(III) complexes have received intense interest as phosphorescent dopants in electroluminescent organic light-emitting diodes (OLEDs)[1,2] since the pioneering studies on *fac*-Ir(ppy)$_3$.[3] The triplet to singlet radiative transition can be promoted by the high spin–orbit coupling associated with the heavy metal atom, leading to complexes that exhibit high phosphorescence quantum yields at room temperature from triplet metal-to-ligand charge-transfer (MLCT) states, relatively short triplet emission decay times and a broad range of emission colours. The photophysical properties of phosphors based on *fac*-Ir(ppy)$_3$ can be tuned by varying the ligands, its substituent groups and/or ancillary ligands.[4–6]

Such complexes are normally used as emitting guests in blends with host materials, where hole-transporting hosts include carbazole derivatives such as CBP [4,4′-di(carbazole-9-yl) biphenyl] and PVK [poly(9-vinylcarbazole)].[7,8] Thus combining Ir(III) complexes with carbazole-based ligands to facilitate hole injection and transport ability in OLEDs has attracted recent attention.[9–16] We reported that OLEDs with the isomeric complexes [2-(Cz-3′-yl)-Py]$_3$Ir **1a** and [2-(Cz-2′-yl)-Py]$_3$Ir **2a** (Scheme 1) as phosphorescent dopants and polyspirobifluorene:bis(triphenyl)diamine (PSBF:TAD) copolymer as host gave green (λ_{max} 500 nm) and orange (590 nm) electroluminescence, respectively, with low external quantum efficiencies (EQEs) of η_{ext} = 0.06% and 1.3%, respectively.[10] The marked difference in the emission energies was ascribed to the different carbazolyl substitution pattern. The low lying triplet level of the host reduced the EQEs by quenching excitons on the dopant complex *via* energy transfer.

There are many reports in the literature on the photophysics of cyclometalated iridium complexes whose ligands are substituted with electron-accepting trifluoromethyl[15–26] or electron-donating methoxy[21,26,27] groups. However, a systematic study of substituent effects on complexes of carbazolyl-pyridine ligands has not been reported until now. The aim of the present work was to synthesise analogues of complexes **1a**[10] and **2a**[10] with a CF_3 or

[a]*Uludag Universitesi, Fen-Edebiyat Fakultesi, Kimya Bolumu, Gorukle Kampusu, 16059 Nilufer, Bursa, Turkey*
[b]*Department of Chemistry, Durham University, Durham DH1 3LE, United Kingdom. E-mail: m.r.bryce@durham.ac.uk*
[c]*Department of Physics, Durham University, Durham DH1 3LE, United Kingdom*

† Electronic supplementary information (ESI) available: Synthetic details and characterisation data for the ligands and complexes; copies of NMR spectra of the new complexes **1b–e**, **2b**,**d**,**e**; computational data. See DOI: 10.1039/c2jm15049b

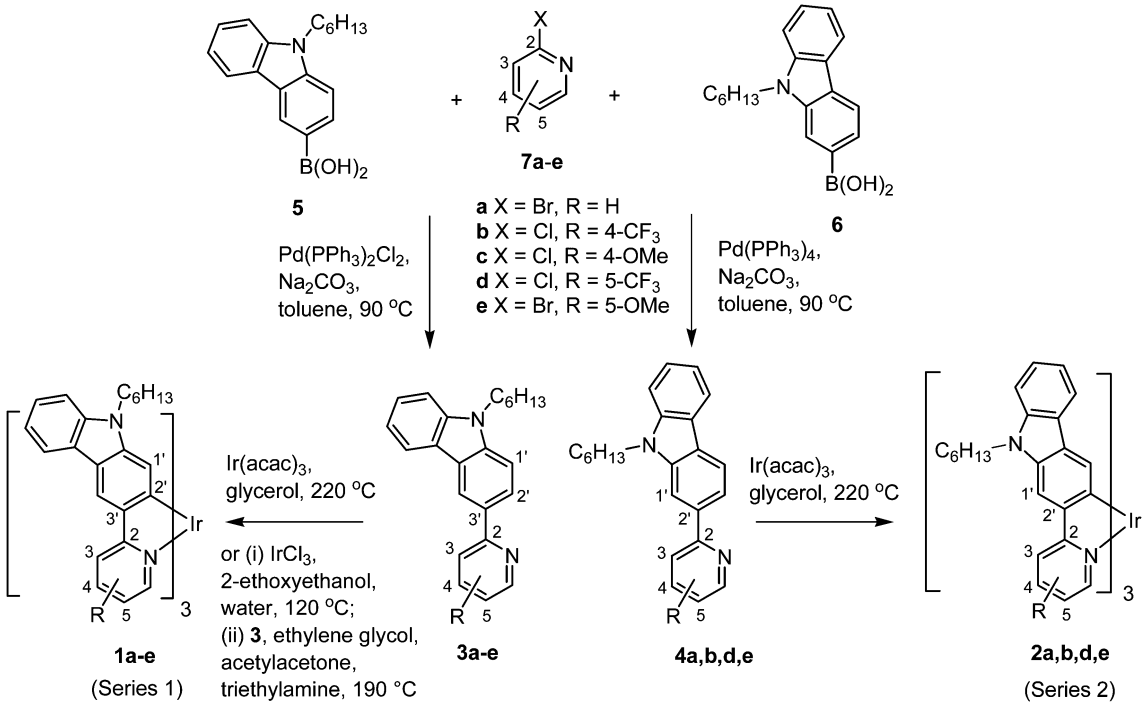

Scheme 1 Synthetic routes to series **1** and **2** complexes.

MeO group attached at various sites on the pyridine ring and to study in detail their electrochemical, photophysical, computational and OLED properties. The two series of complexes **1a–e** and **2a**, **b**, **d**, **e** are described in this article. Colour tuning from green to red of the solution phosphorescence and the electroluminescence has been achieved by substituent effects. High performance has been demonstrated for solution processed OLEDs using these complexes dispersed in PVK as the host polymer.

Results and discussion

Synthetic methodology

Scheme 1 shows the synthetic route to the complexes studied in this article, following our previous protocols for **1a** and **2a**.[9] *N*-Hexylcarbazol-3′-yl and 2′-ylboronic acids **5** and **6**, respectively, underwent standard Suzuki-Miyaura cross-coupling reactions[28] with the 2-halo-4/5-substituted-pyridines, 2-X-4/5-R-Py **7b–e**, to afford the ligands, 2-(Cz-3′-yl)-4/5-R-Py **3b–e** and 2-(Cz-2′-yl)-4/5-R-Py **4b**, **d**, **e**. The ligands were obtained in moderate yields (35–70%) with bis(triphenylphosphine)palladium(II) dichloride, $(PPh_3)_2PdCl_2$, as a catalyst for **3b–e** and tetrakis (triphenylphosphine)palladium(0), $(PPh_3)_4Pd$, as a catalyst for **4b**, **d**, **e**. Following the cyclometalation procedure used for **1a** and **2a**[9] the ligands **3b–e** and **4b**, **d**, **e** were then reacted with $Ir(acac)_3$ in glycerol at 220 °C to give the Ir(III) complexes **1b**, **d**, **e** and **2b**, **d**, **e**. Using this procedure, complex **1c** could not be isolated from **3c**. A different procedure[6] *via* the intermediate diiridium dichloride complex[29] using **3c** and $IrCl_3$ gave **1c** in 70% yield. To establish the generality of this procedure using $IrCl_3$, **1b** was similarly obtained from **3b** using $IrCl_3$ in 51% yield [*cf.* only 2% yield using $Ir(acac)_3$]. The complexes were unambiguously characterised by ^1H and ^{13}C NMR spectroscopy, MALDI-TOF mass spectrometry and elemental analysis. The relative simplicity of the ^1H spectra confirmed the *fac*-isomer structure in each case. No spectroscopic evidence for the *mer*-isomers of these complexes was found. Complex **2c** was not synthesised because the photophysics and device data for **1a** and **1c** are very similar (see below).

Cyclic voltammetry

The CVs of all the complexes studied (**1a**,[10] **b–e** and **2a**,[10] **b**, **d**, **e**) display a cleanly reversible one-electron oxidation wave, with potentials of −0.16 to +0.29 V relative to the ferrocene/ferrocenium couple at 0.00 V, which is assigned to the metal-centered Ir^{III}/Ir^{IV} couple (Table 1). The oxidation potential of **1a** ($E_{1/2}^{ox}$ = 0.06 V) is 0.18 V more positive (*i.e.* lowered HOMO level) than that of **2a** ($E_{1/2}^{ox}$ = 0.36 V), where the carbazole-nitrogen atom is *para* to the metalated Ir-phenyl center. A corresponding value of +0.19 V has been found for the heteroleptic carbazole complexes [2-(Cz-3′-yl)-Py]$_2$Ir(acac) and [2-(Cz-2′-yl)-Py]$_2$Ir(acac) where Cz contains an ethyl group at the carbazole N atoms.[13] A similar value of +0.20 V was reported for [(4′-$Ph_2NC_6H_4$)-Py]$_2$Ir(acac) and [(5′-$Ph_2NC_6H_4$)-Py]$_2$Ir(acac).[5]

The electron withdrawing CF_3 group shifts the oxidation potentials to more positive values (*i.e.* lowered HOMO level) in both series of complexes. The shifts observed are +0.20 and +0.03 V in the sequence **1a** → **1b** → **1d** and +0.17 and +0.03 V in the sequence **2a** → **2b** → **2d**, *i.e.* the oxidation potentials show little dependence on the position of the CF_3 group on the

Table 1 The half-wave oxidation potentials for the Ir^{III}/Ir^{IV} couple ($E_{1/2}^{ox}$, V) and HOMO energies computed for S_0 geometries for both series of Ir(III) complexes

Complex	$E_{½}^{ox}$ (V)[a]	HOMO (eV)[b]	HOMO (eV)[c]
1a	+0.06	−4.86	−4.70
1b	+0.26	−5.06	−5.11
1c	−0.05	−4.75	−4.50
1d	+0.29	−5.09	−5.14
1e	+0.01	−4.81	−4.63
2a	−0.12	−4.68	−4.44
2b	+0.05	−4.85	−4.82
2d	+0.08	−4.88	−4.84
2e	−0.16	−4.64	−4.36
$Ir(ppy)_3$	+0.25	−5.05	−4.84

[a] 0.1 M ($^nBu_4NPF_6$) in dichloromethane at 298 K, scan rate 100 mV s^{-1}, referenced externally to the ferrocene/ferrocenium (FcH/FcH^+) couple. [b] HOMO levels calculated from CV potentials by HOMO = −4.8 + ($-E_{½}^{ox}$), using ferrocene as the standard. [c] HOMO levels calculated from S_0 optimised geometries at B3LYP/LANL2DZ:3-21G*.

pyridine ring. Similar positive shifts (0.18–0.27 V) for heteroleptic Ir(III) complexes with CF_3 groups at the pyridyl rings have been reported elsewhere.[5,19] On the other hand, the electron donating MeO group raises the HOMO level with a shift of $E_{½}^{ox}$ to slightly more negative potentials with a shift of −0.05 and −0.06 in the sequence **1a** → **1e** → **1c**, and −0.04 V for **2a** → **2e**. these data for **1a**, **1c** and **1e** suggest an increased effect of the position of the MeO group (C4 or C5), with an enhanced effect in **1c** where the MeO group is *para* to the iridium atom.

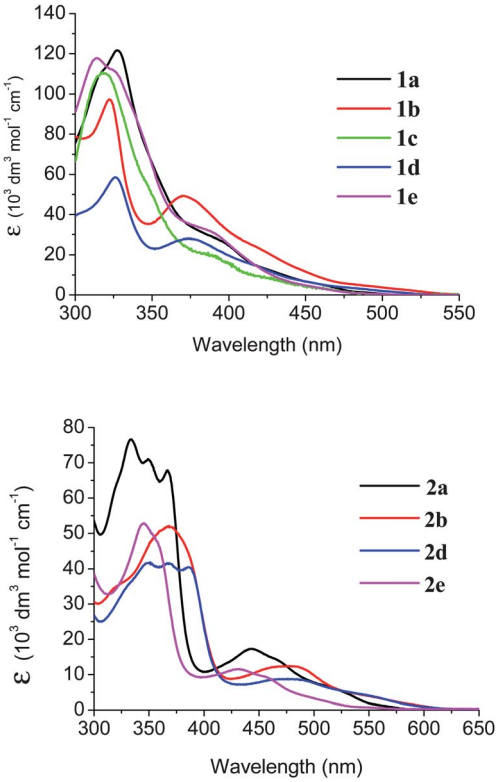

Fig. 1 Molar absorption coefficient spectra for series **1** and **2** complexes showing the differences in the strength, location and the spectral shape of the π–π* and MLCT transitions.

Photophysical data

Absorption. The absorption spectra for the carbazolyl iridium complexes, shown in Fig. 1 and listed in Table 2, contain strong bands assigned to π > π* transitions in the region of 330–300 nm for series **1** complexes and 390–330 nm for series **2** complexes (*vide infra*). While the wavelengths of the strong bands in both series appear to be little affected by MeO groups (**1c**, **1e** and **2e**) there are considerable shifts from the CF_3 groups which result in bathochromic shifts of *ca.* 20 nm for **2b** and **2d** compared to the strong π > π* band in **2a**. A reverse effect is observed in series **1** where the CF_3 groups in **1b** and **1d** cause hypsochromic shifts of *ca* 20 nm with respect to the parent complex **1a**.

The weak bands observed at lower energies than the strong π > π* bands are conventionally assigned to metal-to-ligand charge transfer (MLCT) transitions (*vide infra*). The absorption band ($S_0 > T_1$), corresponding to the lowest energy ^{3}MLCT transition in homoleptic cyclometalated iridium complexes is often very weak and overlapped by close weak bands from many mixed MLCT transitions.[30] In fact, ^{3}MLCT transitions are mixed with ^{1}MLCT transitions on absorption, so a pure $S_0 > T_1$ transition is an arbitrary assignment. Therefore, obtaining accurate $S_0 > T_1$ maxima values from absorption spectra of iridium complexes is unrealistic.[8] Nevertheless, the CF_3 groups in **1b**, **1d**, **2b** and **2d** cause bathochromic shifts of *ca.* 40 nm in these observed weak bands compared to the respective parent complexes, **1a** and **2a**. Small blue shifts can also be seen in the weak MLCT bands due to the MeO group in **1c** compared to **1a**, and in **2e** compared to **2a**.

Emission. The broad featureless bands observed in the phosphorescence spectra in all the complexes in series **1** and **2** (Table 3 and Fig. 2) are characteristic of ^{3}MLCT transitions rather than triplet ligand-ligand transitions.[23] The lower energy shoulders observed in the emission bands of the parent complexes **1a** and **2a** and **1c** are less noticeable in the complexes with CF_3 substituents (**1b**, **1d**, **2b** and **2d**). The metal character in the highest occupied orbitals of these complexes must therefore be substantial, like that for $Ir(ppy)_3$, which has a broad featureless phosphorescence spectrum at room temperature.

By using OMe and CF_3 substituents on the pyridine ring, combined with the two isomeric carbazolyl-pyridine frameworks (series **1** and **2**) the emission colour has been tuned within the range 494–637 nm. It is remarkable that a combination of the electron-withdrawing CF_3 substituent at the pyridyl ring and the electron-donating carbazol-2′-yl substituent, specifically at the *para* position to the iridium atom, gives a bathochromic shift of 128 nm (**2b**) and 124 nm (**2d**) compared to $Ir(ppy)_3$. For some heteroleptic Ir complexes CF_3 substituents on the pyridyl ring give bathochromic shifts of 23–27 nm relative to the parent system,[5,19] whereas larger shifts of 32–54 nm are found here for the carbazole complexes (*i.e.* **1b**, **1d**, **2b**, **2d**, relative to **1a** and **2a**).

On closer inspection, the substitution effects on the emission maxima are intriguing. First consider methoxy substitution. In series **1**, the different positions of the MeO groups cause a blue shift of 10 nm in **1c** and a red shift of 10 nm in **1e**, with respect to **1a**. In contrast to this, in series **2**, the MeO group on **2e** leads to a blue shift of 12 nm, compared to **2a**. Now consider the

Table 2 Absorption data for complexes discussed in this study. All wavelengths are given in nm. Assignments of maxima are based on TD-DFT computations (*vide infra*)

Type	$Ir(ppy)_3$[a]	**1a**[b]	**1b**[b]	**1c**[b]	**1d**[b]	**1e**[b]	**2a**[b]	**2b**[b]	**2d**[b]	**2e**[b]
Edge[c]	510	507	556	500	544	516	592	629	622	581
^{3}MLCT very weak bands	488(2)	481(1)	513(2)	474(1)	500(1)	484(1)	549(1)	581(1)	581(1)	543(1)
^{1}MLCT weak bands	455(3)	457(5)	484(4)	452(3)	476(3)	455(3)	513(5)	546(3)	543(4)	498(3)
	405(8)	429(9)	445(9)	429(6)	445(5)	427(7)	472(10)	503(6)	505(5)	459(7)
	377(12)	400(18)	414(20)	399(11)	413(13)	399(19)	444(13)	478(8)	478(6)	431(9)
	341(9)	378(21)	385(31)	379(14)	384(21)	378(22)	422(9)	455(7)	452(6)	409(6)
		361(21)	365(36)	362(12)	364(19)	362(17)	397(7)	427(6)	424(6)	388(8)
			344(27)		343(19)					
$\pi > \pi^*$ strong bands	283(45)	348(37)	327(51)	348(33)	328(41)	348(35)	367(61)	389(34)	388(37)	361(40)
	244(46)	336(44)	318(57)	336(31)	318(25)	338(41)	348(57)	370(36)	366(31)	345(36)
		326(79)	309(35)	325(71)	309(23)	326(77)	333(63)	356(36)	347(35)	334(30)
		311(83)		311(83)		311(97)	320(52)	342(23)	331(28)	323(24)

[a] In CH_2Cl_2, extinction coefficients (10^3 $dm^3mol^{-1}cm^{-1}$) in parentheses, reference 18. [b] Band maxima and extinction coefficients (10^3 $dm^3mol^{-1}cm^{-1}$) in parentheses estimated from gaussian deconvolution analyses. [c] Red edge of lowest energy band.

effects of CF_3 substitution. In series **1** a CF_3 group at either C4 (**1b**) or C5 (**1d**) causes a red shift, with **1b** exhibiting an enhanced shift of 22 nm compared to **1d**. In series **2**, the significant red shift is again observed, but the positions of the CF_3 groups have only a minimal effect on the emission maxima (difference of only 4 nm between **2b** and **2d**). This indicates that the emission of series **2** is more dominated by the carbazole ligand compared to series **1**. This is supported by the computational calculations below.

The Stokes shifts based on these complexes are remarkably small with values of 0.11–0.20 eV (Table 3) indicating that the excited state geometries do not markedly differ from the ground state geometries. They are characteristic of substantial iridium contributions to the phosphorescence emissions and thus the observed emissions arise from ^{3}MLCT transitions.[6]

The luminescence decays of all complexes in a zeonex matrix at 300 K are in the range of 1.4 μs to 3 μs indicating emission with mixed singlet and triplet character which is characteristic of heavy metal complexes (Table 4).[10,33] The decays of complexes **1a**, **1b**, **1c** and **1d** are all ~1.5 μs (within error limits) but **1e** demonstrates a significantly longer decay time approaching 3 μs. The decays of series **2** complexes are longer and approach 3 μs, except for complex **2b** (1.5 μs). The parent complex **1a** has a lifetime of 1.44 μs in zeonex, which is shorter than our previously reported value of 1.9 μs in degassed toluene at 298 K. We ascribe this to different environments, as similar small discrepancies have been observed previously for $Ir(ppy)_3$. For example, the lifetime for $Ir(ppy)_3$ in N_2-saturated toluene is ~2 μs,[23] in 4,4′-*N*,*N*′-dicarbazolylbiphenyl (CBP) it is ~1.3 μs[34] and in polystyrene matrix it is ~1.2 μs.[35]

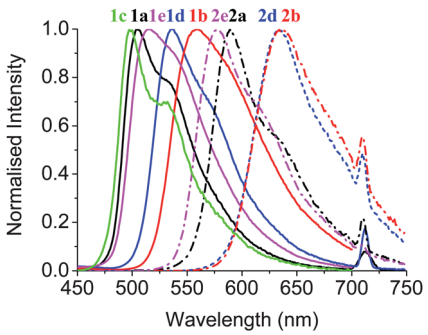

Fig. 2 Normalised phosphorescence spectra for series **1** and **2** complexes in toluene at 298 K. Peaks observed at 710 nm are due to the instrument used (double the excitation wavelength).

Table 3 Photoluminescence (PL) and electroluminescence (EL) emission data for the complexes discussed in this study

Complex	λ_{max} PL (nm)[a]	λ_{max} EL (nm)	TD-DFT (nm) (adjusted)[b]	Stokes shift (eV)[c]
1a	504	506	507	0.12
1b	558	557	556	0.20
1c	494	511	483	0.11
1d	536	540	538	0.17
1e	514	511	517	0.15
2a	589	590	590	0.16
2b	637	627	632	0.18
2d	633	638	641	0.17
2e	577	574	565	0.13
$Ir(ppy)_3$	509	509	509	0.11

[a] PL maxima were measured in toluene; excitation wavelength 355 nm. [b] Scaling factor of 0.925 used on calculated $S_0 > T_1$ energy based on toluene as solvent at 298 K. [c] Calculated from difference between lowest energy band maximum in absorption spectrum and the PL maximum where both spectra are measured in toluene at 298 K.

Table 4 Decay lifetimes and rates measured in an optically inert zeonex matrix at 300 K (τ and $1/\tau$), and radiative (k_r) and non-radiative (k_{nr}) rates calculated using $k_r = \Phi \cdot 1/\tau$ and $k_{nr} = 1/\tau - k_r$. Quantum yields Φ were measured in toluene

	τ, μs[a]	$1/\tau$, s^{-1}	Φ[b]	k_r s^{-1}	k_{nr} s^{-1}
1a	1.44	694000	0.54	375000	319000
1b	1.41	709000	0.45	319000	390000
1c	1.58	633000	0.57[c]	361000	272000
1d	1.65	606000	0.63	382000	224000
1e	2.84	352000	0.35	123000	229000
2a	3.20[d]	313000	0.11	34000	279000
2b	1.53	655000	0.15	98000	557000
2d	2.35	426000	0.10	43000	383000
2e	3.10	323000	0.12	39000	284000

[a] τ error ±10%. Excitation wavelength 355 nm. [b] Assuming a quantum luminescent efficiency yield of $\Phi = 0.40$[31,32] for *fac*-Ir(ppy)$_3$, QY error ±5%. Excitation wavelength 340 nm. [c] QY ±20% and comparing with quinine sulphate ($\Phi = 0.56$) excited at 350 nm. Excitation wavelength for the complex was 425 nm. [d] Taken from ref. 10 in toluene.

The PLQY values are higher for series **1** complexes (0.35 to 0.63) than for series **2** complexes (0.10 to 0.15). Using the quantum yield values one can approximately evaluate k_r and these values are similar for each series of complexes; they are in the order of $\sim 10^5$ s^{-1} for series **1** complexes and $\sim 10^4$ s^{-1} for series **2** complexes. This trend follows a precedent for heteroleptic complexes with similar ligands. The quantum yields for [2-(Cz-3′-yl)-Py]$_2$Ir(acac) and [2-(Cz-2′-yl)-Py]$_2$Ir(acac) (where Cz has an N-ethyl substituent) are 0.22 and 0.02, respectively.[13] The lower PLQYs for series **2** could be due to the increased carbazole ligand contribution to the excited state resulting in decreased radiative decay.

Computational studies

Optimised model geometries (denoted here as **1a′–1e′**, **2a′–2e′**) of the iridium complexes (**1a–1e**, **2a–2e**) with methyl groups in place of hexyl groups at the carbazole nitrogens were used to support the CV and photophysical data. Here we use the B3LYP functional at the LANL2DZ: 3-21G* basis set for series **1** and **2** complexes as a compromise based on comparison between observed and computed data for Ir(ppy)$_3$. The main advantage with this particular model chemistry is that the computing times are considerably shorter than with other model chemistries.

MO computations. Electronic structure calculations carried out on the model S_0 geometries of series **1′** and **2′** iridium complexes show the three HOMO, HOMO−1, HOMO−2 levels (denoted d_2, d_{1a} and d_{1b} for convenience despite dominant ligand character in these occupied orbitals) being similar in energy, and the three LUMO, LUMO + 1, LUMO + 2 (π_1*, π_{2a}* and π_{2b}*) also energetically close, as shown in Fig. 3. They resemble the computed frontier MOs for Ir(ppy)$_3$.[30,36–39]

The orbital energies for **1a′** are remarkably similar to that of Ir(ppy)$_3$ with all frontier orbitals computed at *ca* 0.1–0.15 eV higher in energy. The highest occupied orbital energies for **2a′** are considerably higher than those in Ir(ppy)$_3$ by *ca* 0.4–0.5 eV due to substantial π-electron density contributions from the nitrogen atoms on the carbazole ligands *para* to the iridium atom. The energies of the lowest unoccupied orbitals in **2a′**, however, are similar to those in Ir(ppy)$_3$ thus resulting in a smaller HOMO–LUMO energy gap (HLG) for **2a′** by 0.4 eV compared to Ir(ppy)$_3$ and **1a′**.

Within the composition of the three highest occupied orbitals (HOMO/−1/−2s) for all carbazolyl complexes of series **1′** and **2′**, the metal character is in the region of 34–39% with the carbazole character taking up 53–57% of the orbitals. These orbitals are best described as mixed ligand-metal orbitals (π(cz) + Ir(d) orbitals) with the carbazole character being dominant (Fig. 4). In the occupied orbitals, the carbazole character is increased at the expense of the metal character for series **2′** compared to series **1′** with a difference of 5–10%. The trends in the HOMO energies are reflected in the CV data for these complexes as shown in Table 1 where there are very good correlations within each series.

The three lowest unoccupied orbitals (LUMO/+1/+2s) in **1a′** and **1d′** and in complexes of series **2′** are π*(py + cz) orbitals with mainly pyridyl character. However, the compositions of these orbitals vary with the electron-withdrawing CF_3 group (EWG) and the electron-donating MeO group (EDG) at the 4- or 5-positions. The pyridyl character takes up between 51% (for **2c′**) and 84% (for **1b′**) of these orbitals with the carbazolyl character generally higher in the series **2** complexes than in the series **1** complexes.

Electron-withdrawing CF_3 substituents in **1b′**, **1d′**, **2b′** and **2d′** lower the unoccupied π* orbital energies (LUMO/+1/+2s) by *ca* 0.6–0.7 eV with the energies for the occupied d orbitals (HOMO/−1/−2s) also lower by *ca* 0.4 eV compared to their respective parent complexes **1a′** and **2a′**. Addition of CF_3 groups to the pyridyl rings thus results in substantially smaller HLG energies by *ca* 0.2 eV compared to the parent complexes. Electron-donating MeO substituents in **1c′**, **1e′**, **2c′** and **2e′** have less effect on the orbital energies compared to the parent complexes with raised energies at both frontier orbitals by 0.1–0.2 eV. The different positions of the CF_3 substituent in **1b′** and **1d′** and the MeO group in **1c′** and **1e′** give HLG energy differences of *ca* 0.1 eV. In the series **2** complexes, the substituent positions on the HLG energy differences are less marked.

Computed photophysical data

Absorption. Simulated absorption spectra generated by TD-DFT computations from S_0 geometries were compared with experimental absorption data and assigned accordingly (Table 2 and Fig. 5). The notations ^{1}MLCT and ^{3}MLCT are used due to the absence of spin–orbit coupling in TD-DFT computations when in fact they are mixed ^{1}MLCT and ^{3}MLCT states.[30,36] The occupied metal-containing orbitals involved are mainly of carbazole character. The MLCT transitions involve the three lowest unoccupied π* orbitals (π_1*, π_{2a}*, π_{2b}* = LUMO/+1/+2) and the next three lowest unoccupied π* orbitals (LUMO + 3/+4/+5) resulting in many possible combinations of MLCT transitions. The weak bands observed at long wavelengths in Table 2 thus arise from many singlet and triplet Ir/π(cz) > π*(py) transitions.

The intense bands at *ca* 350 nm observed experimentally are assigned to π > π* ligand-ligand transitions involving the next three highest occupied π orbitals (HOMO+3/+4/+5) which are mainly located at the carbazole rings. These strong transitions in complexes **1a–2e** are therefore described as π(cz) > π*(py) in character.

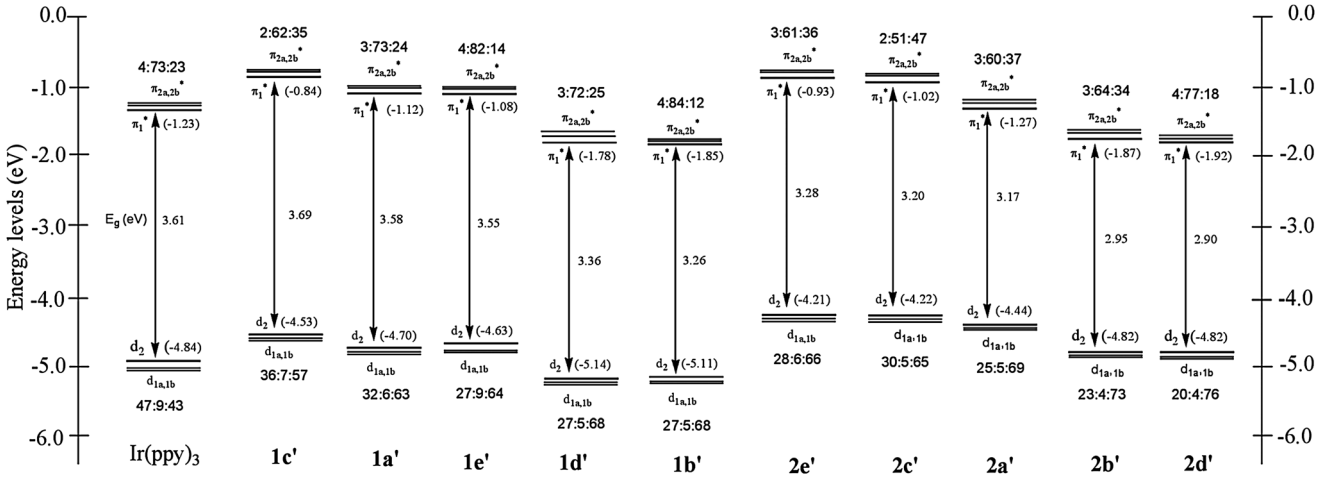

Fig. 3 Schematic drawing of HOMO and LUMO orbital energies of Ir(III) complexes from B3LYP calculations. The values in parentheses correspond to molecular orbital compositions in percentage (%) for the Ir: pyridyl: carbazolyl character averaged from the three orbitals close in energy.

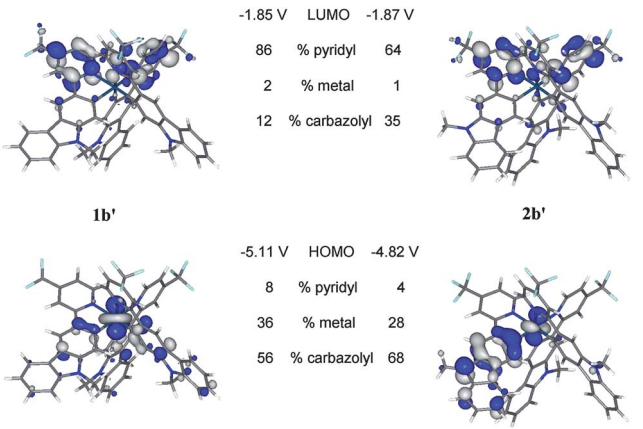

Fig. 4 Frontier orbitals for the model complexes **1b′** and **2b′**. Contour values are plotted at ±0.04 (e/bohr^3).

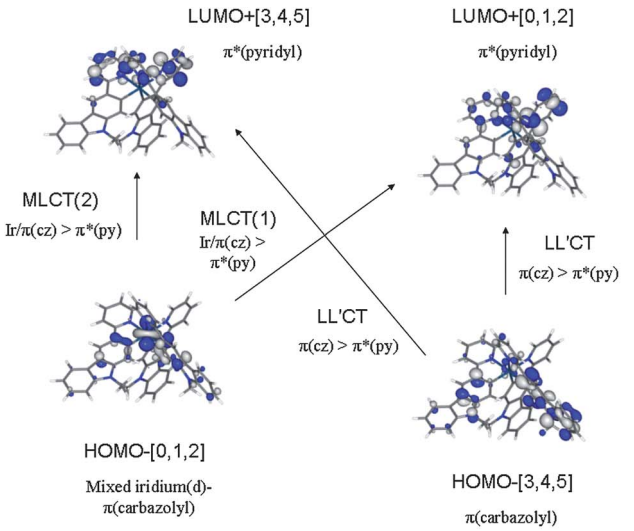

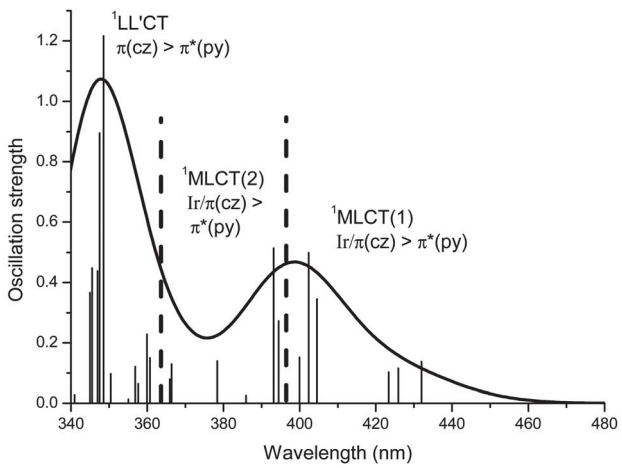

Fig. 5 Molecular orbitals involved in the singlet state ($S_0 > S_n$) transitions and simulated absorption spectrum for **1a′** based on TD-DFT computations.

Emission. As shown experimentally here and elsewhere,[18] the emission properties of iridium complexes are mainly phosphorescence ($S_0 < T_1$) due to fast intersystem crossing (ISC) facilitated by the Ir atom. T_1 geometries for all iridium complexes were optimised here as the TD-DFT data from these geometries would be expected to give more accurate data than TD-DFT data from optimised S_0 geometries. Unlike the near C_3 symmetries for the S_0 geometries, the T_1 optimised geometries for all iridium complexes were of C_1 symmetries with variations of 0.03–0.06 Å for the Ir–C and Ir–N bond lengths.[30,36,38,39] The optimised singlet excited state (S_1) geometries for $Ir(ppy)_3$, **1a′** and **2a′** were also obtained and shown to have similar C_1 symmetries as the T_1 optimised geometries. The S_1 geometries are slightly less stable than the T_1 geometries by 0.08–0.09 eV.

However, the agreement between the PL data and $S_0 > T_1$ transitions from the optimised T_1 geometries is poor with the correlation factor R of 0.973 (Fig. 6). The correlation between the PL data and the HLG data is better at $R = 0.989$! The correlation by comparing energy differences between the SOMO energies from triplet state T_1 and the HOMO energies from singlet state S_0 MO calculations on optimised S_0 geometries

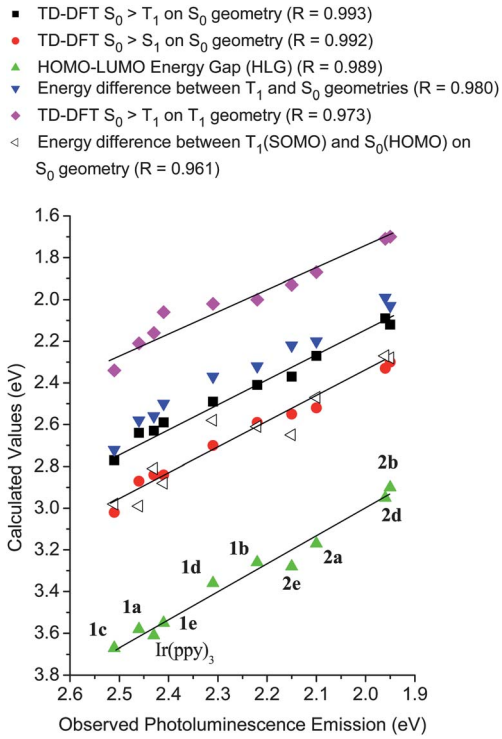

Fig. 6 Correlations between various computed energies and observed PL emission maxima of $Ir(ppy)_3$ and series **1** and **2** complexes.

with observed emission energies reported elsewhere[18,36] is even worse with $R = 0.961$. The predicted Stokes shifts are calculated from the differences between the $S_0 > T_1$ energies of the S_0 and T_1 geometries. They are large at 0.38–0.44 eV compared to Stokes shifts of only 0.11–0.20 eV observed experimentally (Table 3). It appears that the optimised T_1 geometries are not modelled correctly by open-shell DFT calculations for these complexes.

Very good correlations, however, are found between the phosphorescence (PL) data and the computed $S_0 > T_1$ and $S_0 > S_1$ transitions from the optimised S_0 geometries (Fig. 6, $R = 0.993/0.992$). The excellent agreement between the phosphorescence (PL) data and the computed $S_0 > T_1$ transitions from the optimised S_0 geometries suggests that the S_0 geometries for these complexes are more representative as the lowest energy triplet excited state geometries than the optimised T_1 geometries for these complexes. Given that the observed Stokes shifts are very small, the excited state geometries would not be significantly different to the ground state geometries.

For iridium complexes related to $Ir(ppy)_3$ the emission maxima change with temperature and solvent. $Ir(ppy)_3$ has an emission maximum of 510 nm at 298 K and 492 nm at 77 K in 2-methyltetrahydrofuran with an energy difference of 0.09 eV.[18] An emission maximum of 503 nm in cyclohexane and 519 nm in acetonitrile with an energy difference of 0.08 eV is found for the same complex.[26] Despite the difficulties in comparing observed and computed emission maximum for an iridium complex as shown by the changes in the observed emission values and the large energy differences within the different model chemistries, it is highly desirable to predict realistic emission colours from DFT/TD-DFT computations.

A scaling factor may be used for one model chemistry to give more realistic energy values as in the case of observed and computed vibrational energies[40] and NMR shifts[41] elsewhere. A scaling factor of 0.925 is used here for the model chemistry B3LYP/LANL2DZ:3-21G* to give the calculated emission maxima at 298 K in toluene in Table 3. Clearly the agreement between observed and computed data is excellent.

Electrophosphorescent OLED characterisation

The current–voltage characteristics of series **1** and **2** devices are shown in Fig. 7. Series **1** shows higher conductivity for the complexes with CF_3 groups. This is due to the higher transition dipole moments associated with the complexes **1b** and **1d** containing the electron-withdrawing group.[26] In comparison, the parent **1a** and the complexes containing MeO groups **1c** and **1e** show lower hole/electron conductivities. The electroluminescence (EL) emission maxima from these devices are similar to the corresponding photoluminescence (PL) maxima in all complexes as shown in Table 3 and Fig. 8, with energy differences up to only 0.02 eV. These data indicate high colour stabilities of the complexes in these devices. Data are collated in Table 5.

The corresponding device efficiencies plotted as a function of current density (Fig. 9) show that devices with series **1** complexes have higher external quantum efficiencies (EQE) than those of series **2**. However, a direct comparison between the different device efficiencies is not possible due to the photometric method of measuring the device efficiencies. A different colour emitting complex has a different overlap area with the photopic luminosity function, therefore, a simple comparison of their efficiencies is inapplicable. However, all complexes show outstanding device performances since the general device structure consists of only a single spin-coated layer at room temperature and without full-layer thickness optimisation. Devices with complex **1a** have current efficiencies of 40 cd A^{-1} corresponding to an EQE of 12%. These values approach the high values typically found only in multilayer devices constructed using vapour deposition procedures.[42] We should note here that we were unable to correlate the device efficiencies with the complex quantum yields or the rate of radiative k_r within series **1**. This is because in a single-layer device where no electron or hole

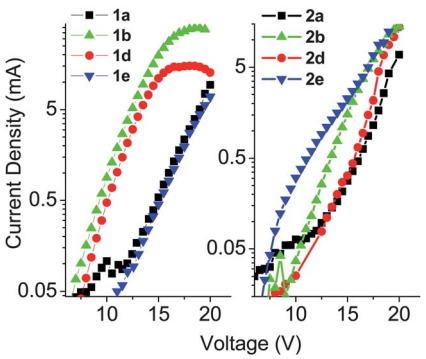

Fig. 7 Current density–voltage characteristics (log-linear plot) for series **1** and **2** complexes in the device structure ITO/PEDOT:PSS-HIL 1.5 (60 nm)/PVK:PBD:Ir complex (90 nm)/Ba (4 nm)/Al (100 nm). Data for **1c** are not shown as they overlap extensively with those of **1a**.

Table 5 Summary of device data

Complex	Turn-on voltage (V) @10 cd m^{-2}	EQE η_{ext} %	Current efficiency (cd A^{-1})	Brightness (cd m^{-2})	Power efficiency (lm/W)
1a	10	12	40	3000	8.5
1b	7	7.9	23.3	2110	7
1c	12	9.2	30.5	2600	7
1d	7.5	10.2	36.5	2980	10
1e	10.5	11.5	36.6	2900	7.5
2a	13	5.6	10.3	120	2
2b	11.5	5.8	4.3	300	1.1
2d	14	4	2.4	110	0.6
2e	10.5	1	1.9	90	0.5

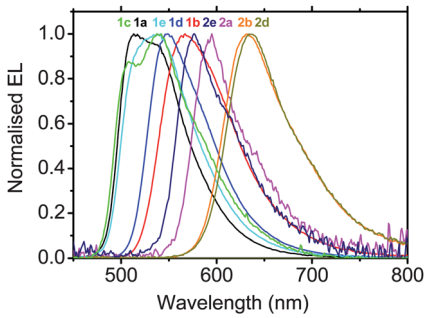

Fig. 8 Normalised electroluminescence spectra (EL) for series **1** and **2** complexes. The distorted vibronic structure near 500 nm for **1a**, **c**, **d**, **e** is due to a device microcavity effect.

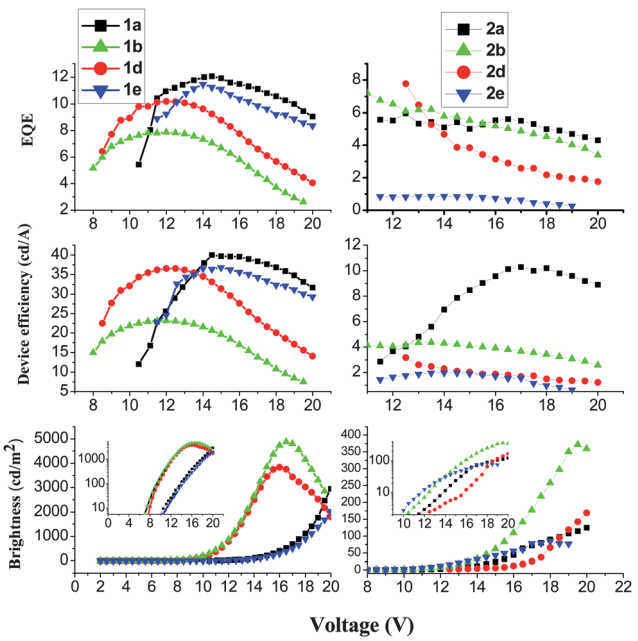

Fig. 9 Efficiencies and brightness for series **1** and **2** complexes in the device structure: ITO/PEDOT:PSS-HIL 1.5 (60 nm)/PVK:PBD:Ir-complex (90 nm)/Ba (4 nm)/Al (100 nm). Data for **1c** are not shown as they overlap extensively with those of **1a**.

blocking layer exists, the device efficiency is dominated by the charge carrier balance (injection and transport) mechanisms rather than by the intrinsic quantum yield of the complex.

Series **2** complexes have lower photoluminescence quantum yields than series **1** complexes in solution (Table 4). This is reflected in lower overall brightness and efficiency in devices fabricated from series **2** in comparison with devices from series **1**. However, within each group of materials the device efficiency and brightness are probably governed by charge transport properties rather than excitonic properties that could be explained by the different molecular dipole moments in each of the materials.

The turn-on voltages of these devices are ≥7 V. A lower turn-on voltage and higher device efficiency would be expected if the blended electron transport material PBD was replaced by a separate evaporated electron-transport/hole-blocking layer, such as TPBi [2,2′,2″-(1,3,5-benzenetriyl)-tris(1-phenyl-1*H*-benzimidazole)] and also if the barium cathode was replaced with LiF. Recent work on a related system has shown that such a multilayer structure enhances electron injection and confines the excitons by blocking the holes, leading to a lower turn-on voltage of 4.1 V.[43] However, our aim in this work is to use a simpler single-active-layer solution-processable structure which is applicable to low-cost, large-area devices and panels for lighting applications.

Conclusions

We have characterised two isomeric series of *fac*-tris-cyclometalated complexes **1a–e** and **2a**, **b**, **d**, **e** which possess carbazolyl-pyridine ligands with the carbazole moieties bonded at the C–3′ and C–2′ positions, respectively. The attachment of a CF_3 or MeO group to the pyridyl ring has been used to tune the colour of the emission for series **1** (λ_{max} PL: 494–558 nm; EL: 506–557 nm) and series **2** (λ_{max} PL: 577–637 nm; EL: 574–638 nm), representing green to red emission. These complexes possess predominantly ^{3}MLCT (metal-to-ligand-charge transfer) excited states. DFT/TD-DFT computations correctly predict their phosphorescence emission maxima and show that the HOMOs in these complexes contain mixed iridium and carbazolyl character. The carbazolyl ligand contributions to the excited states increase in series **2** compared to series **1**. Complexes of series **1** exhibit high phosphorescence quantum yields whereas complexes of series **2** show lower quantum yields. Solution processed OLEDs using series **1** complexes blended in the high triplet poly(9-vinylcarbazole) (PVK) host polymer exhibit very high performances of up to 40 cd A^{-1} and external quantum efficiency of 12%. For series **2** the highest performance is 10.3 cd A^{-1} and

external quantum efficiency of 5.6%. These studies provide new insights into chemically tailoring Ir complexes of carbazolylpyridine ligands, leading to OLEDs with good colour tunability and high efficiencies appropriate for display technologies. The solution processability of these polymer-dopant systems is attractive for the construction of large area devices.

Experimental section

Synthesis of the ligands. Details are given in the ESI.†

Synthesis of the complexes

General procedures. *Route A*: A mixture of the ligand and iridium(acetylacetonate)$_3$ dissolved in degassed glycerol was heated at 220 °C for 65 h under argon. Upon cooling, the mixture was diluted with distilled H_2O and brine solution and then the organic products were extracted into CH_2Cl_2. The combined extracts were dried over $MgSO_4$ and concentrated under reduced pressure to give a crude product which was purified by column chromatography over silica gel. *Route B*: A mixture of the ligand and iridium trichloride in 2-ethoxyethanol: water (3 : 1 v/v) was stirred at 120 °C overnight to yield the intermediate μ-chloro-bridged dimer, which was stirred with the ligand in ethylene glycol, acetylacetone and NEt_3 at 190 °C for 1 h. The mixture was cooled and the precipitated complex was purified by column chromatography over silica gel. Details are given in the ESI.†

Cyclic voltammetry. Cyclic voltammograms were recorded using a BAS CV50W electrochemical analyzer fitted with a three-electrode system consisting of a Pt disk (Ø = 1.8 mm) as the working electrode, a Pt wire as an auxiliary electrode and an Ag/$AgNO_3$ (CH_3CN) as the reference electrode. Experiments were carried out using 0.1 M tetra(n-butyl)ammonium hexafluorophosphate (n-Bu_4NPF_6) solutions in dichloromethane as the supporting electrolyte at a scan rate of 100 mV s^{-1}. The potentials were referenced to the ferrocene/ferrocenium$^+$ redox couple as a secondary external reference.

Photophysical measurements. Solution state photophysical data were obtained using freshly prepared solutions of the complexes in toluene. Emission measurements were taken using thoroughly degassed solutions achieved by repeated freeze-pump-thaw cycles. All measurements were taken using quartz cuvettes with a pathlength of 1 cm. Absorption measurements were taken using an ATI Unicam UV/Vis Spectrometer UV2 (series **1** complexes) or a Perkin Elmer UV/Vis Spectrometer Lambda12 (series **2** complexes). All emission measurements were taken using a Jobin-Yvon Horiba Spex Fluorolog 3 Spectrometer. A right angle illumination method was used and appropriate optical filters were selected to remove 2nd order peaks and Raman scatter.[44] Each spectrum obtained was corrected for the spectral response of the machine. Quantum yields were determined in degassed toluene in comparison with a standard Ir(ppy)$_3$ (0.4) and/or quinine sulfate (0.56). For decay measurements, the complexes were doped in an optically inert zeonex matrix, spincoated onto glass substrates and encapsulated in a nitrogen glovebox to minimize exposure to oxygen. The lifetime measurements were made using a system consisting of an excitation source, pulsed YAG laser emitting at 355 nm (from EKSPLA). Samples were excited at 45° angle to the substrate plane and the energy of each pulse was *ca.* 25 μJ per pulse. Emission was focused onto a spectrograph and detected on a sensitive gated iCCD camera (Stanford Computer Optics) with sub nanosecond resolution. Decay measurements were performed by increasing gate and delay times; more details can be found elsewhere.[45]

OLEDs. All devices were fabricated on indium tin oxide (ITO)-coated glass substrates (VisionTek) of thickness 125 nm and possessing a sheet resistance of 20 Ω/□. The (ITO)-coated substrate was cleaned with acetone and isopropanol, and was treated with ozone for 3 min. Poly(3,4-ethylenedioxy-thiophene) doped with poly(styrenesulfonic acid) (PEDOT:PSS-HIL 1.5), obtained commercially from Bayer A.G. Germany, was spin coated at 2500 rpm for 60 s to produce a *ca.* 40 nm thick hole-transporting layer (HTL). These HTL-coated substrates were then annealed at 200 °C for 2 min to remove any residual water. A chlorobenzene solution of 20 mg mL^{-1} of poly(vinylcarbazole) (PVK) was selected as a high triplet energy host material and as a hole-transport material. The PVK solution was doped with 40% w/w of 2-(4-biphenylyl)-5-(4-*tert*-butylphenyl)-1,3,4-oxadiazole (PBD) as an electron transport material for balancing charge carrier transport. Blended devices were made by mixing 8% w/w of the Ir complexes with the PVK: PBD 40%. The mixture was filtered with a 25 μm pore filter and spin coated at 2500 rpm on top of the PEDOT:PSS layer and baked for 10 min at 120 °C. Each sample was shadow masked to produce two identical devices of area 4 × 12 mm; the samples were then introduced into a nitrogen glove box, where 4 nm barium cathodes were evaporated onto the device at a rate of *ca.* 1 Å s^{-1} under vacuum at a pressure of *ca.* 1 × 10^{-6} mm Hg. This was followed by the deposition of a 150 nm capping layer of aluminium under the same evaporation conditions. The current–voltage (I–V) characteristics and the emission intensities were measured in a calibrated integrating sphere and the data acquisition was controlled using a home-written NI LabView program which controlled the Agilent Technologies 6632B power supply. The electroluminescence (EL) spectra were measured using an Ocean Optics USB 4000 CCD spectrometer supplied with 400 μm UV/Vis fibre optics.

Acknowledgements

We thank EPSRC for funding this work. We thank Heraeus Group for the kind supply of PEDOT:PSS-HIL 1.5 material.

References

1 Reviews: (*a*) Y. You and S. Y. Park, *Dalton Trans.*, 2009, 1267; (*b*) M. S. Lowry and S. Bernhard, *Chem.–Eur. J.*, 2006, **12**, 7970; (*c*) C. Ulbricht, B. Bayer, C. Friebe, A. Winter and U. S. Schubert, *Adv. Mater.*, 2009, **21**, 4418.
2 H. Yersin (Ed.), *Highly Efficient OLEDs with Phosphorescent Materials*; Wiley-VCH, Weinheim, 2008.
3 (*a*) M. A. Baldo, S. Lamansky, P. E. Burrows, M. E. Thompson and S. R. Forrest, *Appl. Phys. Lett.*, 1999, **75**, 4; (*b*) M. A. Baldo, M. E. Thompson and S. R. Forrest, *Nature*, 2000, **403**, 750.
4 (*a*) A. Beeby, S. Bettington, I. D. W. Samuel and Z. Wang, *J. Mater. Chem.*, 2003, **13**, 80; (*b*) C. S. K. Mak, D. Pentlehner, M. Stich, O. S. Wolfbeis, W. K. Chan and H. Yersin, *Chem. Mater.*, 2009,

21, 2173; (*c*) Y. You and S. Y. Park, *J. Am. Chem. Soc.*, 2005, **127**, 12438; (*d*) C. Adachi, M. A. Baldo, M. E. Thompson and S. R. Forrest, *J. Appl. Phys.*, 2001, **90**, 5048; (*e*) S. Jung, Y. Kang, H.-S. Kim, Y.-H. Kim, C.-L. Lee, J.-J. Kim, S.-K. Lee and S.-K. Kwon, *Eur. J. Inorg. Chem.*, 2004, 3415; (*f*) S. Aoki, Y. Matsuo, S. Ogura, H. Ohwada, Y. Hisamatsu, S. Moromizato, M. Shiro and M. Kitamura, *Inorg. Chem.*, 2011, **50**, 806; (*g*) X. Ren, M. E. Kondakova, D. J. Giesen, M. Rajeswaran, M. Madaras and W. C. Lenhart, *Inorg. Chem.*, 2010, **49**, 1301.

5 J. Nishida, H. Echizen, T. Iwata and Y. Yamashita, *Chem. Lett.*, 2005, **34**, 1378.

6 S. Lamansky, P. Djurovich, D. Murphy, F. Abdel-Razzaq, H. E. Lee, C. Adachi, P. E. Burrows, S. R. Forrest and M. E. Thompson, *J. Am. Chem. Soc.*, 2001, **123**, 4304.

7 V. Adamovich, J. Brooks, A. Tamayo, A. M. Alexander, P. I. Djurovich, B. W. D'Andrade, C. Adachi, S. R. Forrest and M. E. Thompson, *New J. Chem.*, 2002, **26**, 1171.

8 K. Brunner, A. van Dijken, H. Börner, J. J. A. M. Bastiaansen, N. M. M. Kiggen and B. M. W. Langeveld, *J. Am. Chem. Soc.*, 2004, **126**, 6035.

9 M. Tavasli, S. Bettington, M. R. Bryce, A. S. Batsanov and A. P. Monkman, *Synthesis*, 2005, 1619.

10 S. Bettington, M. Tavasli, M. R. Bryce, A. Beeby, H. A. Al-Attar and A. P. Monkman, *Chem.–Eur. J.*, 2007, **13**, 1423.

11 W. Y. Wong, C. L. Ho, Z. Q. Gao, B. X. Mi, C. H. Chen, K. W. Cheah and Z. Lin, *Angew. Chem., Int. Ed.*, 2006, **45**, 7800.

12 C. L. Ho, Q. Wang, C. S. Lam, W. Y. Wong, D. Ma, L. Wang, Z. Q. Gao, C. H. Chen, K. W. Cheah and Z. Lin, *Chem.–Asian J.*, 2009, **4**, 89.

13 C. Yang, X. Zhang, H. You, L. Zhu, L. Chen, L. Zhu, Y. Tao, D. Ma, Z. Shuai and J. Qin, *Adv. Funct. Mater.*, 2007, **17**, 651.

14 C. L. Ho, W. Y. Wong, Z. Q. Gao, C. H. Chen, K. W. Cheah, B. Yao, Z. Xie, Q. Wang, D. Ma, L. Wang, X. M. Yu, H. S. Kwok and Z. Lin, *Adv. Funct. Mater.*, 2008, **18**, 319.

15 C. L. Ho, M. F. Lin, W. Y. Wong, W. K. Wong and C. H. Chen, *Appl. Phys. Lett.*, 2008, **92**, 083301.

16 C. L. Ho, W. Y. Wong, Q. Wang, D. Ma, L. Wang and Z. Lin, *Adv. Funct. Mater.*, 2008, **18**, 928.

17 L. S. Hung and C. H. Chen, *Mater. Sci. Eng., R*, 2002, **39**, 143.

18 A. B. Tamayo, B. D. Alleyne, P. I. Djurovich, S. Lamansky, I. Tsyba, N. N. Ho, R. Bau and M. E. Thompson, *J. Am. Chem. Soc.*, 2003, **125**, 7377.

19 (*a*) C. H. Yang, C. H. Chen and I. W. Sun, *Polyhedron*, 2006, **25**, 2407; (*b*) M. L. Xu, M. G. Y. Wang, R. Zhou, Z. W. An, Q. Zhou and W. L. Li, *Inorg. Chim. Acta*, 2007, **360**, 3149.

20 (*a*) Y. H. Park and Y. S. Kim, *Thin Solid Films*, 2007, **515**, 5084; (*b*) A. S. Ionkin, W. J. Marshall, D. C. Roe and Y. Wang, *Dalton Trans.*, 2006, 2468; (*c*) Y. Wang, W. Gao, S. Braun, W. R. Salaneck, F. Amy, C. Chan and A. Khan, *Appl. Phys. Lett.*, 2005, **87**, 193501; (*d*) K. R. J. Thomas, M. Velusamy, J. T. Lin, C. H. Chien, Y. T. Tao, Y. S. Wen, Y. H. Hu and P. T. Chou, *Inorg. Chem.*, 2005, **44**, 5677.

21 I. R. Laskar and T.-M. Chen, *Chem. Mater.*, 2004, **16**, 111.

22 (*a*) V. V. Grushin, N. Herron, D. D. LeCloux, W. J. Marshall, V. V. Petrov and Y. Wang, *Chem. Commun.*, 2001, 1494; (*b*) K. H. Fang, L. L. Wu, Y. T. Huang, C. H. Yang and I. W. Sun, *Inorg. Chim. Acta*, 2006, **359**, 441; (*c*) C. H. Yang, W. L. Su, K. H. Fang, S. P. Wang and I. W. Sun, *Organometallics*, 2006, **25**, 4514.

23 A. Tsuboyama, H. Iwawaki, M. Furugori, T. Mukaide, J. Kamatani, S. Igawa, T. Moriyama, S. Miura, T. Takiguchi, S. Okada, M. Hoshino and K. Ueno, *J. Am. Chem. Soc.*, 2003, **125**, 12971.

24 K. Dedeian, P. I. Djurovich, F. O. Garces, G. Carlson and R. J. Watts, *Inorg. Chem.*, 1991, **30**, 1685.

25 Y. Wang, N. Herron, V. V. Grushin, D. LeCloux and V. Petrov, *Appl. Phys. Lett.*, 2001, **79**, 449.

26 H. A. Al-Attar, G. C. Griffiths, T. N. Moore, M. Tavasli, M. A. Fox, M. R. Bryce and A. P. Monkman, *Adv. Funct. Mater.*, 2011, **21**, 2376.

27 (*a*) I. R. Laskar, S. F. Hsu and T. M. Chen, *Polyhedron*, 2005, **24**, 189; (*b*) F. J. Coughlin, M. S. Westrol, K. D. Oyler, N. Byrne, C. Kraml, E. Zysman-Colman, M. S. Lowry and S. Bernhard, *Inorg. Chem.*, 2008, **47**, 2039; (*c*) S. Okada, K. Okinaka, H. Iwawaki, M. Furugori, M. Hashimoto, T. Mukaide, J. Kamatani, S. Igawa, A. Tsuboyama, T. Takiguchi and K. Ueno, *Dalton Trans.*, 2005, 1583; (*d*) M. L. Xu, T. L. Li, W. L. Li, Z. R. Hong, Z. W. An and Q. Zhou, *Thin Solid Films*, 2006, **497**, 239; (*e*) L. L. Wu, C. H. Yang, I. W. Sun, S. Y. Chu, P. C. Kao and H. H. Huang, *Organometallics*, 2007, **26**, 2017; (*f*) N. Agarwal and P. K. Nayak, *Tetrahedron Lett.*, 2008, **49**, 2710.

28 N. Miyaura and A. Suzuki, *Chem. Rev.*, 1995, **95**, 2457.

29 M. Nonoyama, *Bull. Chem. Soc. Jpn.*, 1974, **47**, 767.

30 K. Nozaki, *J. Chinese Chem. Soc.*, 2006, **53**, 101.

31 K. A. King, P. J. Spellane and R. J. Watts, *J. Am. Chem. Soc.*, 1985, **107**, 1431.

32 Recent literature suggests that the quantum yield for $Ir(ppy)_3$ should be close to 1.00 rather than 0.40: T. Sajoto, P. I. Djurovich, A. B. Tamayo, J. Oxgaard, W. A. Goddard III and M. E. Thompson, *J. Am. Chem. Soc.*, 2009, **131**, 9813.

33 M. Tavasli, S. Bettington, I. F. Perepichka, A. S. Batsanov, M. R. Bryce, C. Rothe and A. P. Monkman, *Eur. J. Inorg. Chem.*, 2007, 4808.

34 Y. Kawamura, J. Brooks, J. J. Brown, H. Sasabe and C. Adachi, *Phys. Rev. Lett.*, 2006, **96**, 017404.

35 W. Holzer, A. Penzkofer and T. Tsuboi, *Chem. Phys.*, 2005, **308**, 93.

36 P. J. Hay, *J. Phys. Chem. A*, 2002, **106**, 1634.

37 E. Jansson, B. Minaev, S. Schrader and H. Ågren, *Chem. Phys.*, 2007, **33**, 157.

38 T. Matsushita, T. Asada and S. Koseki, *J. Phys. Chem. C*, 2007, **111**, 6897.

39 Y. Wu and J.-L. Bredas, *J. Chem. Phys.*, 2008, **129**, 214305.

40 A. P. Scott and L. Radom, *J. Phys. Chem.*, 1996, **100**, 16502.

41 A. E. Aliev, D. Courtier-Murias and S. Zhou, *THEOCHEM*, 2009, **893**, 1.

42 Y. Tao, C. Yang and J. Qin, *Chem. Soc. Rev.*, 2011, **40**, 2943.

43 J.-H. Jou, W.-B. Wang, S.-M. Shen, S. Kumar, I.-M. Lai, J.-J. Shyue, S. Lengvinaite, R. Zostautiene, J. V. Grazulevicius, S. Grigalevicius, S.-Z. Chen and C.-C. Wu, *J. Mater. Chem.*, 2011, **21**, 9546.

44 J. R. Lakowicz, *Principles of Fluorescence Spectroscopy*, Kluwer Academic/Plenum Press, New York, 1999, 2nd Edition.

45 C. Rothe and A. P. Monkman, *Phys. Rev. B: Condens. Matter*, 2003, **68**, 075208.

